COMPUTING METHODS IN APPLIED SCIENCES AND ENGINEERING
R. Glowinski, J.L. Lions (editors)
North-Holland Publishing Company

FLUID DYNAMICS OF THE HEART AND THE EAR

Charles S. Peskin
Courant Institute of Mathematical Sciences
251 Mercer St.
New York, N.Y. 10012

1. Introduction

The aim of this paper is to describe two intriguing problems in the field of physiological fluid dynamics: flow patterns around heart valves and wave propagation in the inner ear. These problems both involve an elastic boundary that is immersed in a viscous, incompressible fluid. These boundaries are the heart valve leaflets and the basilar membrane of the inner ear.

Despite this common physical basis, the fluid dynamics are very different in the two cases. In the heart we have to deal with vortex dynamics in flow at substantial Reynolds numbers, so the problem is highly nonlinear. In the ear, the amplitude of the motion is exceedingly small, so the convection terms of the Navier-Stokes equations can be neglected. Nevertheless, the problem is interesting because of the large variation in stiffness of the basilar membrane from one end to the other.

The research described in this paper has been carried out by the author and his colleagues over a period of several years, and this research program is still very active. Only an overview of this work will be given here, with emphasis on the formulation of the problem and with samples of numerical results. Details of the numerical methods are published elsewhere (see references).

2. Flow patterns around heart valves

a. Physiology

Each ventricle of the heart has an inflow and an outflow valve (see Fig. 2.1). We shall describe the function of these valves on the left side of the heart, but their function on the right side is similar. When the left ventricle is relaxed, its inflow valve (the mitral valve) is open and its outflow (aortic) valve is closed. In this situation the left ventricle forms a common chamber with the left atrium and it receives blood from the left atrium at low pressure (5 mm. Hg.). When the left ventricle contracts, the mitral valve closes and the aortic valve opens. The left ventricle then forms a common chamber with the aorta, and it pumps blood into this artery at high pressure (120 mm. Hg.).

The valves themselves are thin elastic membranes and their motions are primarily determined by the fluid that surrounds them. It is important to realize, however, that the valve leaflets also have a profound influence on the fluid in which they are immersed. This two-way interaction makes the heart-valve problem interesting from a mathematical point of view.

b. Equations of an immersed valve leaflet

In this section we state the equations of motion of a mechanical system that consists of an elastic boundary of zero mass immersed in a viscous incompressible fluid. The region of space occupied by the entire system will be called Ω ; the immersed boundary $B(t)$ moves about in the interior of Ω. We shall write equations of motion that apply on Ω as a whole; this avoids the difficulties of working with the fluid domain $\Omega - B(t)$.

The fluid has density ρ , viscosity μ , velocity $\underline{u}(\underline{x},t)$, and pressure $p(\underline{x},t)$. On account of viscosity, the velocity is continuous across the immersed boundary, and the restriction of $\underline{u}(\underline{x},t)$ to $B(t)$ gives the velocity of the material points of the boundary at time t.

The immersed boundary will be described in parametric form $\underline{X}(s,t)$. When Ω is three-dimensional, s will stand for the pair of parameters (s_1,s_2) and ds will stand for $ds_1 ds_2$. The domain of s will be denoted by B_o. Thus $B(t) = \{\underline{X}(s,t) \mid s \in B_o\}$. The choice of parameters is arbitrary except that fixed s must mark a material point.

Thus we use a Lagrangian description for the immersed boundary

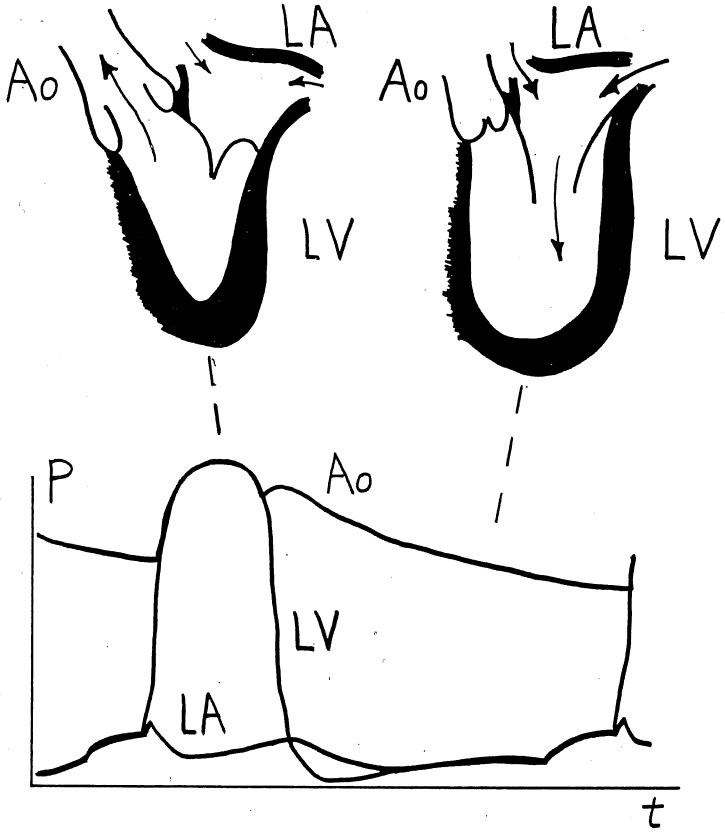

Fig. 2.1 Heart valves and pressures.
LV = Left Ventricle; LA = Left Atrium; Ao = Aorta;
P = Pressure; and t = time.

and an Eulerian description for the fluid. With this notation, the equation of motion may be stated as follows:

$$\rho\left(\frac{\partial \underline{u}}{\partial t} + \underline{u}\cdot\nabla\underline{u}\right) = -\nabla p + \mu\Delta\underline{u} + \underline{F} \tag{2.1}$$

$$\nabla\cdot\underline{u} = 0 \tag{2.2}$$

$$\underline{F}(\underline{x},t) = \int_{B_o} \underline{f}(s,t)\,\delta\big(\underline{x}-\underline{X}(s,t)\big)\,ds \tag{2.3}$$

$$\frac{\partial \underline{X}}{\partial t}(s,t) = \underline{u}\big(\underline{X}(s,t),t\big) = \int_{\Omega} \underline{u}(\underline{x},t)\,\delta\big(\underline{x}-\underline{X}(s,t)\big)\,d\underline{x} \tag{2.4}$$

$$\underline{f}(\ ,t) = S\big(\underline{X}(\ ,t)\big) \tag{2.5}$$

This system of equations is not at all standard, and it requires considerable explanation. Equations (2.1-2.2) are the Navier-Stokes equations for a viscous incompressible fluid with an applied force-density $\underline{F}$. Here we use $\underline{F}$ to represent the force of the immersed boundary on the fluid. It follows that $\underline{F}(\ ,t)$ is a distribution with support on the immersed boundary $B(t)$. (Recall that $\underline{F}$ has units of force/volume, but the boundary exerts a finite force in zero volume.)

The explicit form of $\underline{F}$ is given in Eq. (2.3) in which $\delta(\underline{x})$ stands for $\delta(x)\delta(y)\delta(z)$. The integration in Eq. (2.3) does not completely remove the singularity since the dimension of the boundary is one less than the dimension of Ω. In our numerical method, therefore, $\underline{F}$ will be $O(h^{-1})$ and the volume of its support will be $O(h)$.

The exact meaning of $\underline{f}(s,t)$ can be found by integrating Eq. (2.3) over an arbitrary region $\Omega_1 \subset \Omega$. The result is

$$\int_{\Omega_1} \underline{F}(\underline{x},t)\,d\underline{x} = \int_{B_1} \underline{f}(s,t)\,ds \tag{2.6}$$

where $B_1 = \{s\,|\,\underline{X}(s,t) \in \Omega_1\}$.

Thus $\underline{f}$ is the density of the boundary force with respect to the boundary element ds, and Eq. (6) asserts that the force of the boundary on the region Ω_1 can be attributed to the part of the boundary that lies in Ω_1. In other words, the boundary force acts locally in the fluid.

Despite the local nature of the boundary force, its effects are felt instantaneously throughout the incompressible fluid. To see how this comes about, take the divergence of both sides of Eq. (2.1). The result is

$$\Delta p = -\rho\underline{u}\cdot\nabla\underline{u} + \nabla\cdot\underline{F} \tag{2.7}$$

Thus $\nabla\cdot\underline{F}$ acts as a source of the pressure field.

Eq. (2.4) simply asserts that the boundary moves at the local fluid velocity; here, we regard this as an equation of motion of the boundary and not as a constraint on the fluid velocity. The second equality in Eq. (2.4) is just the definition of the δ-function, which we write out to emphasize a certain symmetry with Eq. (2.3). Together, Eqs. (2.3) and (2.4) express the interaction between the boundary and the fluid, and the δ-function appears as a kernel in both cases. As remarked above, this expresses the local nature of the interaction.

Eq. (2.5) makes the important assertion that the boundary force is determined by the boundary configuration. This is a consequence of our assumptions that the boundary is elastic and massless. To illustrate this point, consider a two-dimensional example in which the boundary is an elastic curve (Fig. 2.2). Let s measure arc length in the unstressed configuration, let $\underline{\tau}$ be the unit tangent to the curve, and let T be the boundary tension. Then

$$\underline{\tau} = \frac{\partial \underline{X}/\partial s}{|\partial \underline{X}/\partial s|} \tag{2.8}$$

$$T = \sigma\big(|\partial \underline{X}/\partial s| - 1\big) \tag{2.9}$$

Consider an arc (a,b) of the boundary. Since the boundary has zero mass, the total force on this arc must be zero:

$$-\int_a^b \underline{f}\,ds + T\underline{\tau}\Big|_a^b = 0 \tag{2.10}$$

Fig. 2.3 Comparison of theory and experiment. Computed results are shown in (a,c) and experimental results from the laboratory of E. L. Yellin in (b,d). The two flow traces in (a) correspond to flow at the mitral ring and flow at the tips of the leaflets. The experimental flow (b) is measured at the ring only.

Fig. 2.2 Boundary force. T = Tension; $\underline{\tau}$ = unit tangent; X(s,t) = boundary configuration at time t. The forces at the ends of arc (a,b) are transmitted to the fluid along that arc.

In Eq. (2.10), the first term is the force of the fluid on the arc (a,b) and the second term is the force of the rest of the boundary on this arc. Since a and b are arbitrary, this shows that

$$\underline{f} = \frac{d}{ds}(T\underline{\tau}) \tag{2.11}$$

Substituting (2.8) and (2.9) in (2.11), one can obtain an explicit example of the kind of relationship that is summarized by Eq. (2.5).

The system of equations (2.1-2.5) is remarkable in that the fluid stress tensor evaluated at the boundary never appears explicitly. As we have just seen, this is a direct consequence of the massless character of the boundary. If the boundary were massive, then we would need an equation for its acceleration. This equation would involve the sum of the elastic and fluid forces on an element of the boundary, and there would be no way to avoid explicit reference to the fluid stress tensor.

c. Computer test chamber for prosthetic mitral valves

We have discretized equations (2.1)-(2.5) to obtain a numerical method for the heart valve problem (Peskin, 1972, 1975, 1977; Peskin and McQueen, 1980). Since the details of the method have already been published, only its use will be considered here.

We use the method to solve the equations of motion of blood in a two-dimensional model of the left heart. The model has a left atrium and a left ventricle with contractile walls that have the physiological properties of heart muscle. The model heart is floating in fluid, so its walls as well as its valves are modeled as immersed boundaries. There is a source in the atrium that corresponds to pulmonary venous return, and there is a sink around the edges of the domain that accepts the volume displaced as the heart fills.

At the junction of the atrium and ventricle, we mount a model mitral valve, natural or artificial. With the natural valve in place, we adjust the physiological properties of heart walls until the results are in reasonable agreement with animal experiments as judged by records of presure and flow as functions of time. The comparison is shown in Fig. 2.3. In this figure all scales are the same except that the flow curves have been scaled arbitrarily on account of the difficulty of comparing three-dimensional flow (volume/time) with two-dimensional flow (area/time). The computed streamlines of the natural

mitral valve are shown in Fig. (2.4).

Once we have established physiological conditions, we are in a position to test artificial valves in the computer and conduct parametric studies on the design of artificial valves. In Figs. (2.5)-(2.7) we show the computed flow patterns of a ball valve, and two pivoting disc valves.

The pivoting discs differ only in the position of the pivot point, and we do not impose any constraint on the maximum angle of opening. We find, however, that this angle depends on the position of the pivot point so that the valve in Fig. (2.7) opens much less than the valve in Fig. (2.6). This illustrates how the method can be used for parametric studies.

The principal limitations of this work are that the model is two-dimensional and that our numerical experiments are conducted at low Reynolds number. The Reynolds number appropriate for dog hearts (where heart valve experiments are often done) is about 500. Our numerical results were obtained at a Reynolds number of 20. As mentioned above, the computed and experimental results appear to agree despite this discrepancy. Nevertheless, it would be desirable to remove this limitation.

d. Vortex methods

A high Reynolds number method for the incompressible Navier-Stokes equation is the vortex method of A. J. Chorin (1973), and we conclude this discussion with a brief description of some papers that apply this method to the heart valve problem. In the thesis of Mendez (1977), a new method for the creation of vorticity at an immersed, elastic boundary is introduced. This method can be derived by taking the curl of Eq. (2.3) and noticing that each element of the boundary force acts as a source of a vortex dipole. In Peskin and Wolfe (1978), the vortex method is combined with conformal mapping and used to study the formation of the aortic sinus vortex. The use of conformal mapping avoids the difficulty of solving Laplace's equation numerically to compute the potential part of the flow. It also provides high resolution near corners where the slip velocity may be infinite. In McCracken and Peskin (1980), a vortex-grid method for the problem of blood flow in the heart is introduced. In this method, vorticity is stored either in the form of moving vortex blobs or on a fixed computational mesh. Tangential forces create vortex dipoles which are retained only for a fixed number of time steps; then their vorticity is transferred to the mesh.

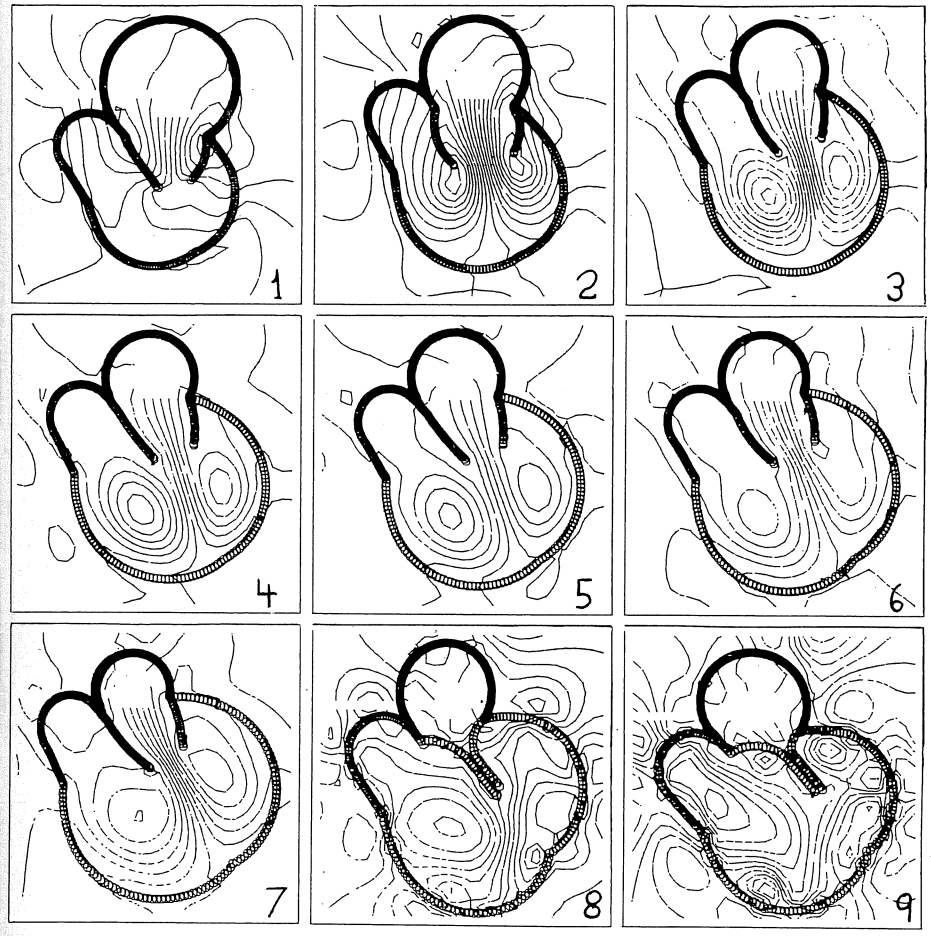

Fig. 2.4 Streamlines of the natural mitral valve at equally spaced times. (Note that streamlines cross moving boundaries.) In (1), the ventricle is relaxing and the valve is opening. Vortex formation occurs in (2) and establishes the characteristic flow pattern of ventricular filling. Contraction of the atrium strengthens the jet in (6-7). Valve closure has just begun in (7); it is completed by contraction of the ventricle in (8).

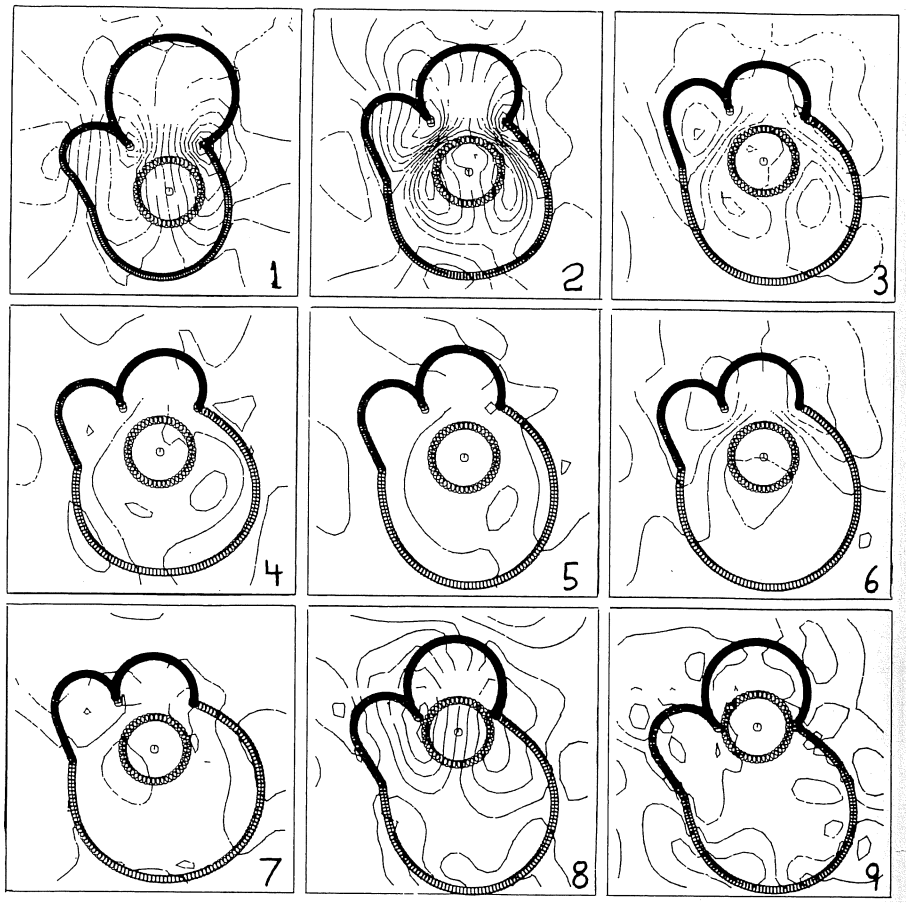

Fig. 2.5 Streamlines of a caged ball valve. Note the distinction between the flow pattern when the ball is opening (1) and after it has reached the open position (2). Similarly compare the closing flow pattern (8) with the closed flow pattern (9). As long as the ball is moving it is not an obstacle to the flow.

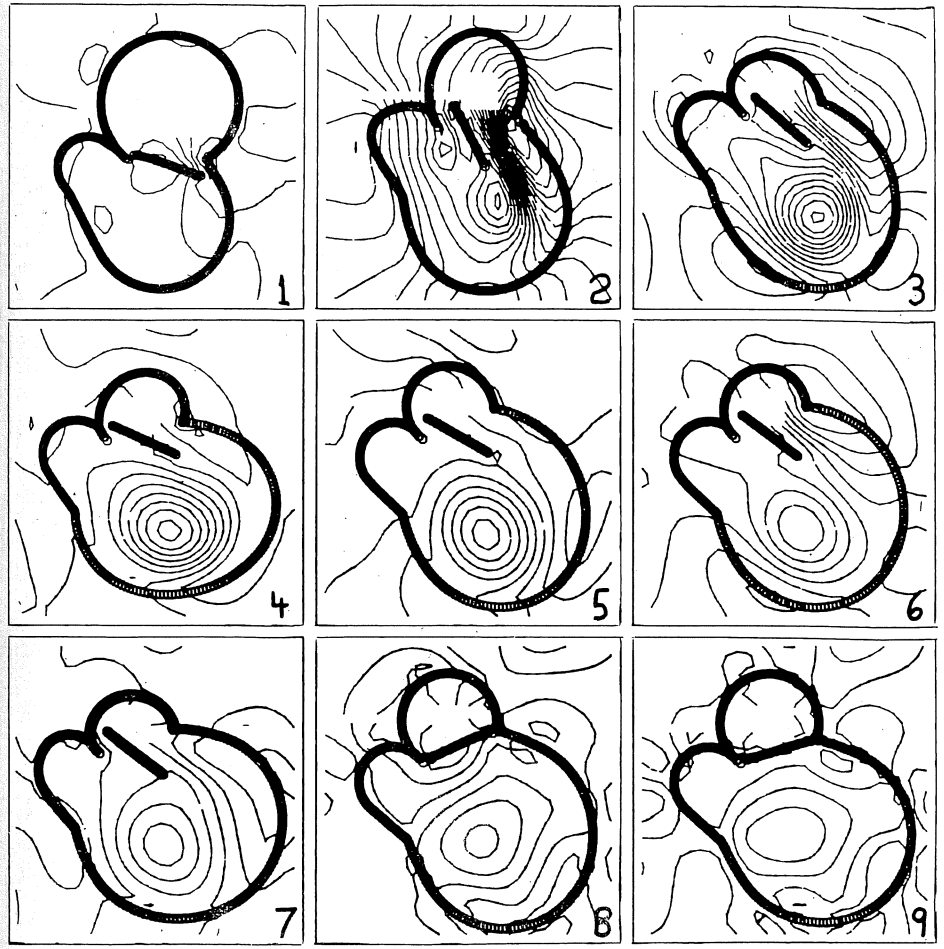

Fig. 2.6 Streamlines of a pivoting disc valve. In This computation, we impose no mechanical constraint on the angle of opening, which is set by the fluid dynamics. Our purpose is to study the effect of the position of the pivot point on the angle of opening (compare Fig. 2.7).

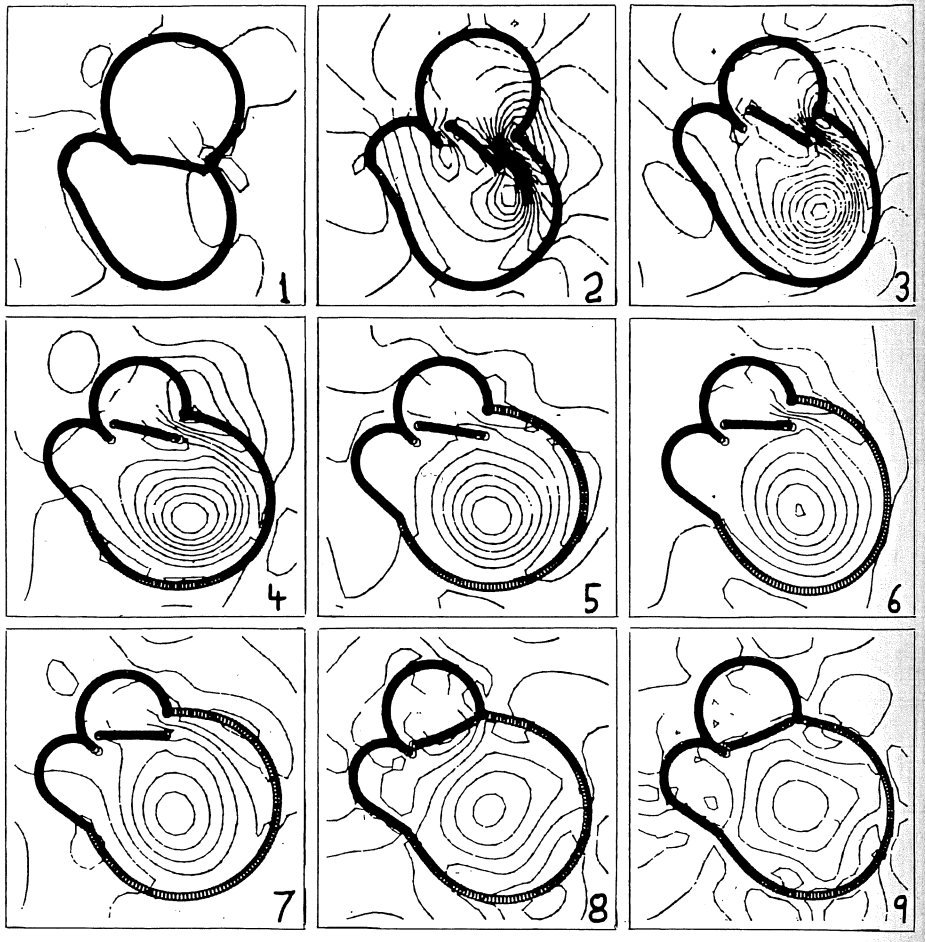

Fig. 2.7 Effect of moving the pivot point. The valve in this figure is identical to the valve in Fig. 2.6 except that the pivot point has been moved closer to the center of the valve. The angle of opening is substantially less than before.

3. Fluid dynamics of the inner ear

a. Physiology

The inner ear (cochlea) is a cavity in the temporal bone of the skull. Unlike the outer and middle ear, which are filled with air, the cochlea is filled with an essentially incompressible fluid. An elastic structure, the basilar membrane, runs along the length of the cochlea and divides it into two main parts. The wave motions that occur in the cochlea propagate along the basilar membrane. Although they occur in response to sound, these disturbances are not sound waves in the ordinary sense. Instead, they are vibrations in which the mass of an incompressible fluid is coupled to the elasticity of an immersed boundary. The kinetic energy of these waves is entirely a property of the fluid and the potential energy is entirely a property of the elastic boundary.

The physiology of the cochlea as we understand it today was first elucidated by George von Bekesy (1960). Using static tests with a constant pressure difference, von Bekesy discovered the important fact that the stiffness of the basilar membrane decreases exponentially with distance into the cochlea. Von Bekesy also studied the pattern of vibration of the basilar membrane in response to a pure tone (sine wave). His method was to observe the motions of the basilar membrane directly using a microscope with stroboscopic illumination. Von Bekesy found that the response of the ear to a steady pure tone takes the form of a wave. The points of constant phase propagate into the ear at a velocity that decreases with distance. The amplitude of the wave is a steady function of position that rises gradually to a unique maximum and then decays rapidly on the far side of this maximum. The point of maximum amplitude varies as the negative logarithm of the frequency of the stimulating sound. In fact, when the frequency of the sound is changed the whole pattern of vibration translates to a new position without much change in form. This correspondence between frequency and position (the cochlea map) is important because the fibers of the auditory nerve are distributed along the length of the basilar membrane. Thus each nerve fiber responds best to a particular frequency, and a complex sound is transmitted to the brain with its different frequency components carried along different nerve fibers. This is an important aspect of the mechanism of separating signals from noise in hearing.

It should be mentioned that the problem of constructing a theory to account for these observations has attracted the attention of many

investigators (Lesser and Berkley, 1972; Siebert, 1974; Steele, 1974; Inselberg and Chadwick, 1976; Cole and Chadwick, 1977, Allen, 1977; Steele and Taber, 1979a, 1979b).

Nevertheless, the work that will be described here (see also Peskin, 1976, and Isaacson, 1979) is different in the following respects. First, we show how a simple conformal mapping can be used to reduce the inviscid cochlea problem to a standard water-wave problem. Second, we show how the corresponding viscous problem can be reduced to an integral equation on the basilar membrane, and we give two numerical methods for solving this integral equation.

b. Two-dimensional model

The model that we shall use is shown in Fig. 3.1. The boundaries at $y = \pm a$ are rigid, and the model is unbounded in the positive and negative x-direction. The moving boundary corresponding to the basilar membrane is described by the unknown function $y = h(x,t)$. We assume that the displacements of all fluid particles are small, so we neglect the non-linear terms in the Navier-Stokes equation, and we apply the boundary conditions appropriate for $y = h(x,t)$ to the undisturbed position of the basilar membrane which is $y = 0$.

We assume that the fluid is incompressible with density ρ and viscosity μ. The fluid velocity and pressure will be denoted (u,v) and p.

The equations of the model are as follows

$$\rho \frac{\partial u}{\partial t} + \frac{\partial p}{\partial x} = \mu \Delta u \tag{3.1}$$

$$\rho \frac{\partial v}{\partial t} + \frac{\partial p}{\partial y} = \mu \Delta v + f(x,t)\delta(y) \tag{3.2}$$

$$\frac{\partial u}{\partial x} + \frac{\partial v}{\partial y} = 0 \tag{3.3}$$

$$f(x,t) = -s_o e^{-\lambda x} h(x,t) \tag{3.4}$$

$$\frac{\partial h}{\partial t}(x,t) = v(x,0,t) \tag{3.5}$$

$$u(x,0,t) = 0 \tag{3.6}$$

$$u(x,\pm a,t) = v(x,\pm a,t) = 0 \tag{3.7}$$

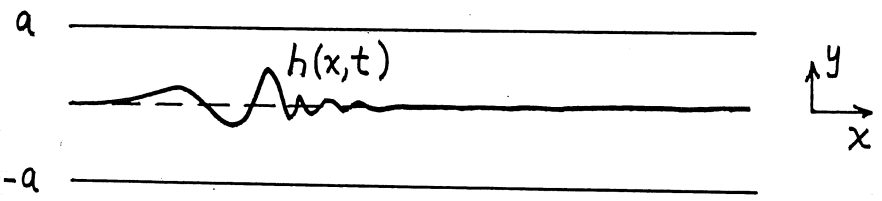

Fig. 3.1 The model cochlea

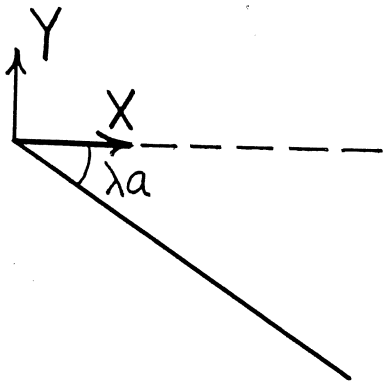

Fig. 3.2 The transformed problem. The conformal mapping given by Eqs. (3.14)-(3.16) takes the lower half-cochlea into the wedge shown here. The inviscid cochlea problem is equivalent to gravity waves on a sloping beach with the source at the beach and the waves going out.

In these equations f(x,t) corresponds to the force per unit length exerted by the basilar membrane on the fluid. The resulting pressure difference across the membrane can be found by integrating (3.2) across y=0. The result is

$$[p] = \mu[\frac{\partial v}{\partial y}] + f \tag{3.8}$$

when [ ] denotes the jump in a quantity across y=0. From (3.3) and the boundary condition $u=0$ at $y=0$, we see that $\partial v/\partial y = 0$ on both sides of the membrane. Therefore

$$[p] = f = -s_o e^{-\lambda x} h \tag{3.9}$$

where we have used (3.4).

Equation (3.4) contains the physics of the model basilar membrane. According to this equation, the basilar membrane has zero mass, and it exhibits linear elastic behavior at each x with a spring stiffness of the form $s_o e^{-\lambda x}$. The exponential dependence of stiffness on position comes directly from the static measurements of von Bekesy (1960). The reader should notice that the different points of the basilar membrane are not coupled to each other by Eq. (3.4). That is, there are no terms involving the space derivatives of h. This comes about because the real basilar membrane is narrow and supported along its edges, see Peskin (1976).

Finally, we have to discuss how the model cochlea is driven. The real cochlea is excited at the stiff end by the piston-like action of two elastic membranes, one of which is connected to the eardrum by a chain of tiny bones. These two membranes are on opposite sides of the basilar membrane, and one moves out while the other moves in so that the total volume of the cochlea is conserved. In the model we assume that there is a sinusoidal source (with the appropriate antisymmetry) at $x = -\infty$. In a careful treatment of the problem, this would be built into the boundary conditions, but we shall be deliberately vague on this point since the details of how the cochlea is driven have very little effect on the form of the wave that results. Some reasons for this will appear below.

c. The inviscid case ($\mu=0$)

In this section we study the behavior of our model cochlea when $\mu=0$. In this case it is reasonable to look for potential flow solutions in which $(u,v) = \text{grad } \phi$. Because of the antisymmetry in the way

that the cochlea is driven, it is also reasonable to look for solutions that satisfy

$$\phi(x,y,t) + \phi(x,-y,t) = 0 \tag{3.10}$$

Under these conditions, our equations reduce to the following system in the strip $-a \le y \le 0$:

$$\frac{\partial^2 \phi}{\partial t^2} + \frac{s_o e^{-\lambda x}}{2\rho} \frac{\partial \phi}{\partial y} = 0, \qquad y = 0 \tag{3.11}$$

$$\Delta \phi = 0, \qquad -a < y < 0 \tag{3.12}$$

$$\frac{\partial \phi}{\partial y} = 0 \qquad y = -a \tag{3.13}$$

The boundary condition at the basilar membrane (3.11) was obtained from (3.9) by differentiating with respect to time and using the relations $\rho \partial\phi/\partial t + p = 0$, $\partial h/\partial t = (\partial\phi/\partial y)_{y=0}$, and $[\phi] = -2\phi_{y=0^-}$.

Equations (3.11)-(3.13) are very nearly the same as the equations for gravity waves of small amplitude in a channel of finite depth. The only difference between the two cases is that here the role of the gravitational constant g is played by the coefficient $s_o e^{-\lambda x}/2\rho$, which depends on x. We can get rid of this space-dependence, however, by applying the conformal mapping

$$X = e^{\lambda x} \cos \lambda y \tag{3.14}$$

$$Y = e^{\lambda x} \sin \lambda y \tag{3.15}$$

which can also be written

$$Z = e^{\lambda z} \tag{3.16}$$

where $z = x + iy$ and $Z = X + iY$. This mapping takes the strip $-a < y < 0$ into the wedge $-\lambda a < \arg(Z) < 0$. Along $y = 0$, we have

$$\frac{\partial \phi}{\partial y} = \lambda e^{\lambda x} \frac{\partial \Phi}{\partial Y} \tag{3.17}$$

so that our problem becomes

$$\frac{\partial^2 \Phi}{\partial t^2} + \frac{s_o \lambda}{2\rho} \frac{\partial \Phi}{\partial Y} = 0 \qquad Y = 0, \quad X > 0 \tag{3.18}$$

$$\Delta \Phi = 0 \qquad -\lambda a < \arg(Z) < 0 \tag{3.19}$$

$$\frac{\partial \Phi}{\partial N} = 0 \qquad -\lambda a = \arg(Z) \tag{3.20}$$

where $\partial\Phi/\partial N$ stands for the normal derivative. Note that the factor $e^{-\lambda x}$ has disappeared and that we have transformed our problem into the problem of gravity waves on a sloping beach (see Fig. 3.2). In our case, the source is at the shoreline and the waves go out, because $x = -\infty$ maps into $X=Y=0$.

We do not need a detailed solution to this problem. Instead we can look at the behavior for large X. If the source has time-dependence $e^{i\omega t}$, then this will generate a wave that propagates away from the shoreline. For large X this wave looks like

$$\Phi(X,Y,t) = e^{i(\omega t-kX)}e^{kY} = e^{i(\omega t-kZ)} \tag{3.21}$$

where

$$k = \frac{2\rho\omega^2}{s_o\lambda} \tag{3.22}$$

Note that (3.21) satisfies (3.18) and (3.19) exactly, but not (3.20). Nevertheless (3.20) is satisfied approximately for large X because of the exponential decay as $Y \to -\infty$. Note also that our approximate solution is independent of the depth of the original cochlea model. It is also independent of the details of how the cochlea is driven.

Transforming back to the coordinates of the cochlea model, we find

$$\phi(x,y,t) = e^{i(\omega t-ke^{\lambda z})} \tag{3.23}$$

To find the vertical velocity we evaluate

$$\frac{\partial\phi}{\partial y}(x,y,t) = Ae^{i\theta} \tag{3.24}$$

where

$$A = k\lambda e^{(\lambda x+ke^{\lambda x}\sin\lambda y)} \tag{3.25}$$

$$\theta = \omega t - ke^{\lambda x}\cos\lambda y + \lambda y \tag{3.26}$$

For $y = 0$ we have simply

$$A = k\lambda e^{\lambda x} \tag{3.27}$$

$$\theta = \omega t - ke^{\lambda x} \tag{3.28}$$

According to these expressions, both the amplitude and the spatial frequency $(-\partial\theta/\partial x)$ of the basilar membrane velocity blow up exponentially as $x \to \infty$. This pathological behavior is a consequence of leaving viscosity out of the model. Nevertheless, we find something interesting if we examine the solution at a fixed depth $-\lambda y = \delta > 0$. Then the amplitude A has the form

$$A = k\lambda e^{(\lambda x-ke^{\lambda x}\sin\delta)} \tag{3.29}$$

which has a unique maximum at x_p given by

$$\lambda x_p = \log\frac{1}{k\sin\delta} \tag{3.30}$$

The expressions for A and θ can be written more simply in terms of $x - x_p$ as follows

$$A = \frac{\lambda}{\sin\delta}e^{(r-e^r)} \tag{3.31}$$

$$\theta = \omega t - \delta - \frac{e^r}{\tan\delta} \tag{3.32}$$

where

$$r = \lambda(x - x_p) \tag{3.33}$$

This result is sketched in Fig. 3.3. At any finite depth, then, the solution is very well-behaved. The amplitude A given by (3.31) rises exponentially for $r << 0$, achieves it maximum at $r=0$ $(x=x_p)$, and decays very rapidly $(\sim\exp(-\exp(r)))$ for $r >> 0$. The spatial frequency still blows up exponentially but this is not a serious problem since the amplitude is decaying so rapidly. These results are consistent with the pathological behavior when $y=0$ because $x_p \to \infty$ as $y \to 0$.

Perhaps we can use this inviscid solution to get an idea how the model basilar membrane will behave when the fluid viscosity is small but not zero. By "small" fluid viscosity we mean that the boundary layer thickness $(\mu/\rho\omega)^{\frac{1}{2}}$ is small compared to λ^{-1}. In these circumstances we expect the inviscid solution to be valid outside the boundary layer and we can get a rough idea of what the basilar membrane is doing by evaluating the inviscid solution at the "edge" of the boundary layer. This motivates setting $y = -(\mu/\rho\omega)^{\frac{1}{2}}$ so that $\delta = \lambda(\mu/\rho\omega)^{\frac{1}{2}}$. By assumption, δ is small, so we set $\sin\delta = \delta$ in (3.30).

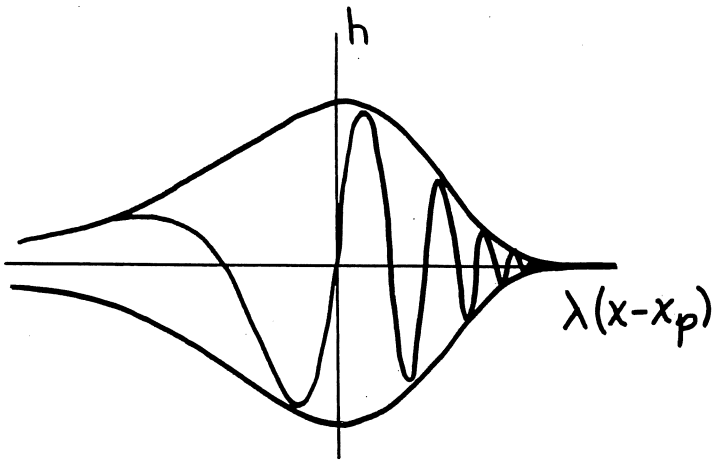

Fig. 3.3 Form of the cochlea wave as calculated by evaluating the inviscid solution at the edge of the viscous boundary layer. The direction of propagation is from left to right. Note the asymmetry of the envelope, which decays much more rapidly to the right than to the left. The spatial frequency increases exponentially from left to right.

Recalling the formula for k (3.22) we find the following expression for the cochlea map

$$\lambda x_p = -\frac{3}{2}\log\frac{\omega}{\omega_o} \tag{3.34}$$

where $\omega_o = (s_o^2/4\rho\mu)^{1/3}$.

We are now in a good position to discuss the physics of the cochlea wave under conditions of small viscosity. The waves in the cochlea are concentrated near the basilar membrane with a depth of penetration into the fluid that is roughly equal to the local wavelength. The wavelength decreases as the wave propagates into the cochlea, however, so the depth of penetration decreases and the amplitude rises as the energy of the wave is compressed against the basilar membrane. When the wavelength becomes less than the boundary layer thickness, however, essentially all of the energy is in the viscous boundary layer and the amplitude of the wave decays rapidly. Thus the point of maximum amplitude occurs near the place where the wavelength and boundary layer thickness are equal. This condition determines the form of the cochlea map.

d. The viscous case: reduction to an integral equation

In this section we return to the viscous problem (3.1)-(3.7) and we consider solutions that are harmonic in time. These solutions satisfy a certain integral equation for the basilar membrane displacement. The derivation of this integral equation proceeds as follows:

First, express all quantities in terms of their complex amplitudes, e.g., let

$$h(x,t) = \mathrm{Re}\left(H(x)e^{i\omega t}\right) \tag{3.35}$$

Next, take the Fourier transforms in the x-direction, e.g., let

$$\hat{H}(\xi) = \frac{1}{\sqrt{2\pi}}\int_{-\infty}^{\infty} h(x)e^{-i\xi x}dx \tag{3.36}$$

After these manipulations, the fluid equations (3.1-3.3 with boundary conditions 3.5-3.7) become a system of ordinary differential equations in y with ξ as a parameter. These equations can be solved explicitly for a relationship between $\hat{H}$ and $\hat{F}$ of the form

$$\hat{H}(\xi) = -\hat{K}(\xi)\hat{F}(\xi) \tag{3.37}$$

where

$$\hat{K}(\xi) = \frac{1}{2}\frac{\xi}{\rho\omega^2\alpha}\frac{2\alpha\xi(1-\cosh\,\xi a\,\cosh\,\alpha a)+(\alpha^2+\xi^2)\sinh\,\xi a\,\sinh\,\alpha a}{\alpha\,\cosh\,\xi a\,\sinh\,\alpha a-\xi\,\sinh\,\xi a\,\cosh\,\alpha a} \tag{3.38}$$

$$\alpha = \sqrt{\xi^2+\frac{i\omega\rho}{\mu}} \tag{3.38a}$$

When $a = \infty$, this expression simplifies as follows:

$$\hat{K}(\xi) = \frac{1}{2}\frac{|\xi|}{\rho\omega^2}\left(1-\frac{1}{\sqrt{1+\frac{i\omega\rho}{\mu\xi^2}}}\right) \tag{3.38b}$$

which behaves like $|\xi|$ for small $|\xi|$ and like $|\xi|^{-1}$ for large $|\xi|$.

From (3.4) we also have

$$F(x) = -s_o e^{-\lambda x}H(x) \tag{3.39}$$

To combine these equations, we introduce the following operator notation

$$F = \text{Fourier transform} \tag{3.40}$$

$$E = \text{Multiplication by } e^{-\lambda x} \tag{3.41}$$

$$\hat{K} = \text{Multiplication by } \hat{K}$$

Note that F is unitary, so $F^* = F^{-1}$. Taking the Fourier transform of (3.39) and substituting in (3.37), we find

$$\hat{H} = s_o\hat{K}FEF^*\hat{H} \tag{3.43}$$

which can also be written

$$H = s_o F^*\hat{K}FEH \tag{3.44}$$

we can think of (3.44) as an eigenproblem for the operator $F^*\hat{K}FE$, which is not self-adjoint. Suppose we have found an eigenfunction H corresponding to some eigenvalue s_o^{-1}. It is easy to check that the translates

of H are also eigenfunctions corresponding to different values of s_o. In this way we can show that the spectrum of $F^*\hat{K}FE$ contains the positive real axis if it contains any point on that axis. We can therefore prescribe s_o arbitrarily and try to determine H. For numerical purposes it is useful to state this problem in least-squares form: Find H subject to

$$\int_{-\infty}^{\infty}|H|^2dx = 1 \tag{3.45}$$

that minimizes

$$\int_{-\infty}^{\infty}|H - s_oF^*\hat{K}FEH|^2\,dx \tag{3.46}$$

e. Two numerical methods for the viscous problem

The methods that will be outlined here were developed by Peskin (1976) and Isaacson (1979). Both are based on the least-squares formulation (3.45)-(3.46). Upon discretization, this leads to the problem of finding an eigenvector corresponding to the smallest eigenvalue of A*A, where A is the matrix that arises from the discretization of $(I - s_oF^*\hat{K}FE)$. Such an eigenvector can be found by the inverse power method

$$A^*Aw^{n+1} = w^n / \|w^n\| \tag{3.47}$$

The two methods of this section use different discretizations, however, and they solve (3.47) in different ways.

In Peskin's method, the problem is discretized by introducing a mesh of N equally spaced points on the x-axis and a similar mesh on the ξ-axis. The mesh-widths are chosen as

$$\lambda\Delta x = \frac{\Delta\xi}{\lambda} = \left(\frac{2\pi}{N}\right)^{\frac{1}{2}} \tag{3.48}$$

so that $\Delta x\,\Delta\xi = 2\pi/N$, and

$$e^{-ix_j\xi_k} = e^{-i(j\Delta x)(k\Delta\xi)} = e^{-i\frac{2\pi}{N}jk} \tag{3.49}$$

Then the operator F is replaced by the discrete Fourier transform of

order N, which has matrix elements, given by (3.49). The multiplication operators $\hat{K}$ and E are replaced by the appropriate diagonal matrices.

The matrix A*A that results from this process of discretization is not sparse, but this matrix is not needed explicitly, since (3.47) is solved using the subroutine package SYMMLQ (Paige and Saunders, 1973), which is a variant of the conjugate gradient method. This method needs the matrix of the system to be solved only in the form of a subroutine which can multiply this matrix by an arbitrary vector. In our case, multiplication by A*A can be broken down into a sequence of steps which are Fast Fourier Transforms or multiplication by diagonal matrices. Thus we can multiply by A*A in O(N log N) operations and solve our linear systems in $O(N^2 \log N)$ operations, since N multiplications by A*A are required. (In practice scaling is required to achieve the solution in N steps; see Peskin, 1976, for details.)

Some computational results obtained using this method are shown in Fig. 3.4. These results are for the simplest case which is $a = \infty$.

In Isaacson's method, discretization of (3.45)-(3.46) is achieved by means of the Rayleigh-Ritz procedure with the Hermite functions as an orthonormal basis. That is, the minimization is performed over the subspace of L_2 that is spanned by the first N Hermite functions. Note that the Hermite functions are eigenfunctions of the Fourier transformation.

It turns out that a good solution can be computed for moderate values of N, so Isaacson computes the matrix elements of A*A explicitly and uses the Cholesky factorization in the solution of (3.47). In computing the matrix elements, Isaacson uses Gauss-Hermite quadrature, and he takes advantage of the following identity

$$(FEH)(\xi) = \hat{H}(\xi - \lambda i) \qquad (3.50)$$

The expression $\hat{H}(\xi-\lambda i)$ always makes sense when $\hat{H}$ is a linear combination of Hermite functions, since the Hermite functions are entire functions.

In practice Isaacson's method is much faster than Peskin's because a comparable solution can be achieved with a much smaller value of N. Therefore his method was used to compute the form of the cochlea wave at several frequencies for a realistic finite depth and to construct a numerical cochlea map for the viscous problem. This map is plotted in Fig. (3.5).

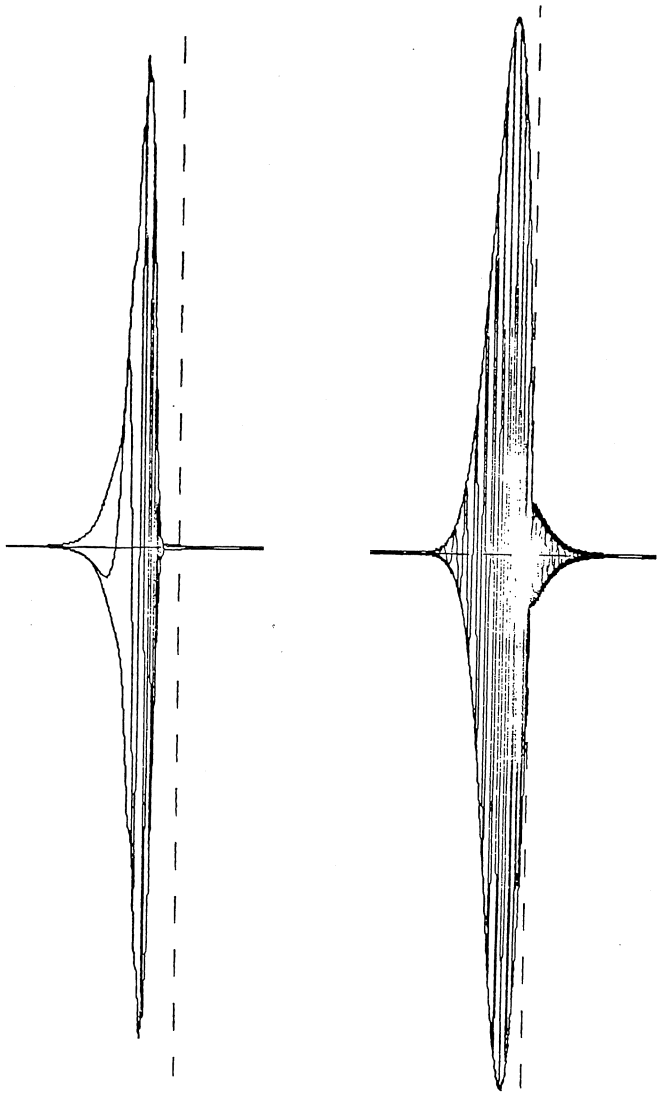

Fig. 3.4 The cochlea wave (left) and its Fourier transform (right). In the cochlea wave, note the gradual rise and rapid fall of the envelope as well as the increasing spatial frequency of the wave. In the Fourier transform note the predominance of negative frequencies which correspond to waves moving from left to right. This occurs despite the absence of any explicit reference to a source at $x = -\infty$ in the computation.

Acknowledgments

The author is indebted to the following individuals for their contributions to the work reported in this paper: Edward Yellin, Alexandre Chorin, Olof Widlund, David McQueen, Marjorie McCracken, Antoinette Wolfe, and Eli Isaacson.

The work on heart valves was supported by the National Institutes of Health (U.S.A.) under research grant HL-17859. Computation was also supported in part by the Department of Energy (U.S.A.) under contract EY-76-C-02-3077 at the Courant Mathematics and Computing Laboratory of New York University. Travel was supported by the NSF (U.S.A.).

References

Allen, J.B. (1977). "Two-dimensional cochlear fluid model: New results," J. Acoust. Soc. Am. 61, 110-119.

Bekesy, G. (1960) Experiments in Hearing (E.G. Weaver, trans.), McGraw Hill, New York.

Chorin, A.J. (1973). "Numerical study of slightly viscous flow," J. Fluid Mech. 57, 785-796.

Cole, J.D., and Chadwick, R.S. (1977). "An approach to mechanics of the Cochlea," ZAMP 28, 785-804.

Inselberg, A., and Chadwick, R.S. (1976). "Mathematical Model of the Cochlea," SIAM J. Appl. Math. 30, 149-179.

Isaacson, Eli (1979). A Numerical Method for a Finite-Depth, Two-Dimensional Model of the Inner Ear. Thesis, NYU (Mathematics), 1979.

Lesser, M.B., and Berkley, D.A. (1972). "Fluid mechanics of the cochlea. Part I," J. Fluid Mech. 51, 497-512.

McCracken, M.F., and Peskin, C.S. (1980). "A Vortex Method for Blood Flow Through Heart Valves," J. Comput Phys. (to appear).

Mendez, R. (1977). Numerical Study of Incompressible Flow in a Region Bounded by Elastic Walls. Thesis, U.C. Berkeley (Mathematics).

Paige, C.C., and Saunders, M.A. (1973). "Solutions of Sparse Indefinite Systems of Equations and Least Squares Problems" (report: STAN-CS-73-399) Stanford University (Computer Science).

Peskin, C.S. (1972). "Flow Patterns Around Heart Valves: A Numerical Method," J. Comput. Phys. 10, 252-271.

-- (1975). Mathematical Aspects of Heart Physiology Courant Institute Lecture Notes.

-- (1976). Partial Differential Equations in Biology Courant Institute Lecture Notes, Ch. 5.

-- (1977). "Numerical Analysis of Blood Flow in the Heart," J. Comput. Phys. 25, 220-252.

Peskin, C.S., and McQueen, D.M. (1980). "Modeling Prosthetic Heart Valves for Numerical Analysis of Blood Flow in the Heart," J. Comput. Phys. (to appear).

Peskin, C.S. and Wolfe, A.W. (1978). "The Aortic Sinus Vortex," Federation Proceedings 37, 2784-2792.

Siebert, W.M. (1974) "Ranke revisited -- a simple short-wave cochlear model," J. Acoust. Soc. Am. 56, 594-600.

Steele, C.R. (1974). "Behavior of the basilar membrane with pure tone excitation," J. Acoust Soc. Am. 55, 148-162.

Steele, C.R., and Taber, L. (1979a). "Comparison of WKB and Finite Difference Calculations for a Two-Dimensional Cochlear Model," J. Acoust. Soc. Am 65, 1001-1006.

-- (1979b). "Comparison of WKB Calculations and Experimental Results for Three-Dimensional Cochlear Models," J. Acoust. Soc. Am. 65, 1007-1018.

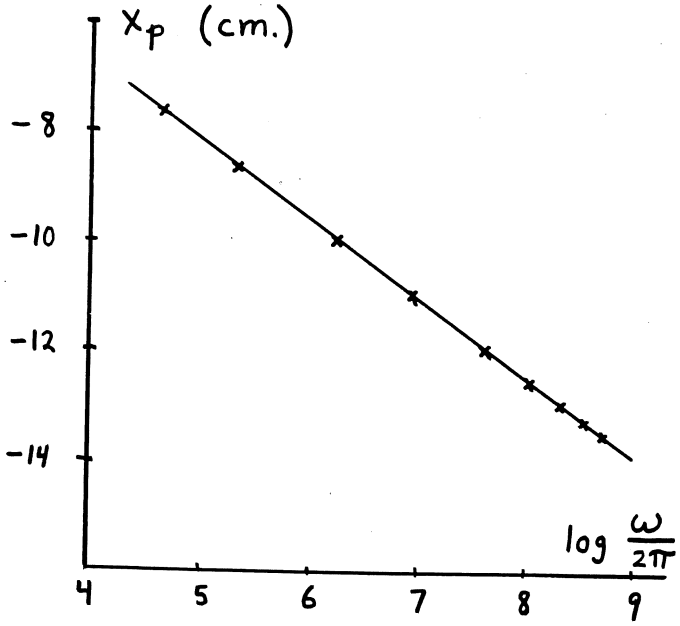

Fig. 3.5 The cochlea map (from the thesis of Eli Isaacson). The computations apply to the viscous, finite-depth case with the following parameters: $a = 0.2$ cm, $\mu = 0.02$ (cm^2/sec)$\cdot$(gm/cm^3), $\rho = 1.0$ gm/cm^3, $\lambda = 1.4$ cm^{-1}.